

Sea ice melt drives vertical pCO₂ variability modulating air-sea gas exchange

Henry C. Henson^{1,2}, Dorte H. Søgaard^{2,3,7}, Bjarne Jensen⁶, Kunuk Lennert⁴, Tim Papakyriakou⁵, Mikael K. Sejr^{1,2}, Jakob Sievers⁶, Søren Rysgaard^{2,7}, and Lise Lotte Sørensen^{2,6}

¹Department of Ecoscience, Aarhus University, Aarhus, 8000, Denmark

²Arctic Research Center, Aarhus University, Aarhus, 8000, Denmark

³Greenland Climate Research Cluster, Greenland Institute of Natural Resources, Nuuk, 3900, Greenland

⁴UiT, The Arctic University of Norway, Tromsø, 9037, Norway

⁵Centre for Earth Observation Science, University of Manitoba, Winnipeg, MB, R3T 2N2, Canada

⁶Department of Environmental science, Aarhus University, Roskilde, 4000, Denmark

⁷Department of Biology, Center for Ice-free Arctic Research, Aarhus University, Aarhus, 8000, Denmark

Corresponding author: Henry C. Henson (hch@ecos.au.dk)

Key Points:

- Spring melting of sea ice and snow introduces distinct heterogeneity in surface water conditions within coastal Arctic oceans.
- Standard bulk parameterizations for air-sea CO₂ flux calculations, based on subsurface pCO₂ measurements, may misrepresent flux direction and magnitude during melt periods.
- Vertical near-surface temperature and CO₂ gradients must be considered to improve flux estimates in stratified Arctic fjords.

30 **Abstract**

31 Strong spatial and temporal gradients in salinity, temperature, and carbonate chemistry in Arctic
32 coastal surface waters complicate the estimation of air-sea carbon dioxide (CO₂) exchange,
33 particularly during sea ice breakup. This study evaluates the applicability of the widely used bulk
34 flux model under such conditions. The bulk approach assumes homogeneous surface conditions
35 and no vertical pCO₂ gradients in the bulk seawater. However, our observations in a stratified
36 Arctic fjord reveal pronounced vertical variability in pCO₂ within the upper water column,
37 including non-linear gradients near the air-sea interface. Micrometeorological flux estimates
38 suggested variability in the direction of gas transfer, even when waters at 1 m depth and below
39 were CO₂-undersaturated. We hypothesize that transient, high-pCO₂ layers within the upper
40 decimeters intermittently decouple the atmospheric exchange from subsurface waters and have
41 the potential to reverse the expected flux direction. These findings highlight the importance of
42 resolving near-surface variability during the transition from ice-covered to open water
43 conditions. We recommend incorporating micrometeorological techniques and high-resolution
44 vertical profiling in Arctic fjords to improve flux estimates of CO₂ in this rapidly changing
45 region.

46 **Plain Language Summary**

47 Sea ice melt adds less-saline water to the surface ocean. This creates vertical gradients in
48 salinity, temperature, and partial pressures of carbon dioxide (pCO₂). The concentration
49 difference of pCO₂ across the air-ocean boundary is used to estimate gas transfer. Thus, the
50 depth that we measure will impact our estimates. Directly measuring gas transfer showed both
51 CO₂ uptake and release from the ocean during sea ice breakup. This means ocean layering during
52 ice melt may briefly reverse the direction of CO₂ transfer.

53 **1 Introduction**

54
55 High latitude coastal oceans are strong sinks for atmospheric carbon dioxide (CO₂), absorbing
56 more CO₂ per unit area than lower latitude regions (Dai et al., 2022; Roobaert et al., 2019). This
57 strong uptake results from both the high solubility of gases in cold water and the intense
58 biological activity typical of these regions. However, climate change is rapidly transforming this
59 carbon sink. The Arctic is warming more than twice as fast as the global average, and sea ice
60 extent has been shrinking by over 13% per decade (Perovich et al., 2020). The loss of sea ice
61 increases CO₂ uptake by exposing larger areas of open water for longer periods, which can
62 further stimulate biological productivity (Arrigo and van Dijken, 2015; Bates and Mathis, 2009;
63 Perovich et al., 2020). However, at the same time, melting sea ice freshens the surface layer and
64 strengthens stratification, limiting vertical mixing with deeper water. Freshwater from melting
65 sea ice and terrestrial run-off creates pronounced gradients in physical properties such as salinity
66 and temperature, as well as chemical properties like dissolved inorganic carbon (DIC) and total
67 alkalinity (TA) (e.g. Henson et al., 2025). As a result, the partial pressure of CO₂ (pCO₂) can
68

69 vary markedly with depth under melt conditions (Miller et al., 2019).

70

71 This vertical variability in pCO_2 poses a challenge for air-sea CO_2 flux estimation. The transfer
72 of gases between the atmosphere and ocean depends on the difference in concentration between
73 the two as well as the efficiency of the transfer process. Therefore, the bulk flux of CO_2 across
74 the air-sea interface is commonly described as the product of the gas transfer velocity, k ($m\ s^{-1}$),
75 CO_2 solubility s ($mol\ kg^{-1}\ atm^{-1}$), and the partial pressure gradient (μatm) across the air-sea
76 interface (Wanninkhof et al., 2009):

77

$$78 \quad F = ks(pCO_{2_{sea}} - pCO_{2_{air}}) \quad (1)$$

79

80 While widely applied, this formulation simplifies a complex process influenced by surfactants on
81 the water surface, bubble-mediated gas exchange, and turbulence (Wanninkhof et al., 2009).
82 Furthermore, surface water heterogeneity, driven by sea ice melt and freshwater runoff from
83 land, complicate the physical and chemical processes governing air-sea CO_2 exchange. As a
84 result, simplified parameterizations commonly used in global carbon flux estimates may be
85 inadequate in these settings.

86

87 In most studies, pCO_2 is measured several meters below the surface, assuming vertical
88 homogeneity under well-mixed condition (Jørgensen et al., 2020). However, in stratified waters,
89 where temperature, salinity, and pH can vary with depth, this assumption may lead to substantial
90 errors in flux estimates (Ahmed et al., 2020; Dong et al., 2021; Miller et al., 2019; Watts et al.,
91 2022). Although Arctic surface waters are often undersaturated with respect to atmospheric CO_2
92 levels and act as CO_2 sinks (e.g., Burgers et al., 2017; Dai et al., 2022; Henson et al., 2024;
93 Laruelle et al., 2014; Roobaert et al., 2019), such assessments typically rely on sparse data
94 collected from 0.5-5 m depth during limited periods. Dong et al. (2021) illustrate that high
95 latitude fluxes of CO_2 calculated using the bulk method (based on measurements sampled at 6 m
96 depth) differ significantly from those measured using direct eddy covariance in sea ice melt
97 regions.

98

99 Gas transfer velocity (k) is often parameterized as a function of wind speed. However, the true
100 driver is mixing in the surface waters, which governs k . Fick's first law of diffusion, which
101 underlies Equation (1), assumes a linear concentration gradient within the diffusive sublayer
102 (Fig. 1) and steady-state conditions (Garbe et al., 2014). Jørgensen et al. (2020) argued that, due
103 to seawater's high buffer capacity, chemical gradients do not significantly affect CO_2
104 equilibration, supporting the use of measurements at 3-4 m depth. However, this conclusion
105 relies on the assumption of horizontal and vertical homogeneity and neglects the effects of
106 shallow surface stratification, particularly when alkalinity dilution is involved.

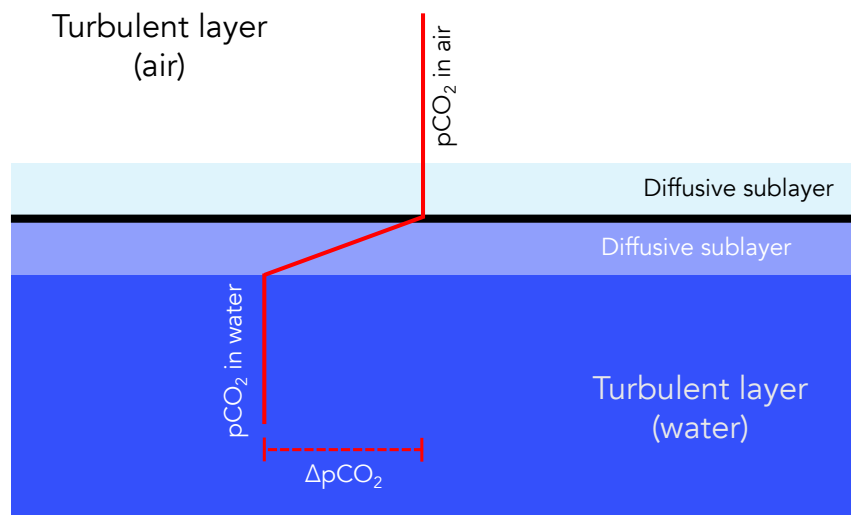
107

108 In Arctic spring, the upper ocean is often strongly stratified due to freshwater input from glacier
109 melt, snowmelt, river runoff, and sea ice meltwater (Ahmed et al., 2020; Granskog et al., 2011;
110 Meire et al., 2017; Miller et al., 2019). These inputs can extend vertical CO_2 gradients beyond
111 the diffusive sublayer, complicating flux estimates during ice break-up and early open-water
112 periods. Several studies have demonstrated strong vertical heterogeneity in pCO_2 in Arctic
113 coastal waters, with implications for air-sea flux calculations (Ahmed et al., 2020; Dong et al.,
114 2021; Miller et al., 2019).

115 Surface freshening from ice melt and runoff strongly influences carbonate chemistry in Arctic
116 coastal waters, which can either suppress or enhance oceanic CO_2 uptake. For example, Burgers
117 et al. (2017) reported large horizontal variability in surface pCO_2 (144–364 μatm) linked to
118 riverine input in the Eastern Canadian Arctic. Similarly, Sejr et al. (2011) observed strong
119 surface pCO_2 gradients associated with salinity and temperature in Young Sound, and later
120 documented a long-term decline in surface salinity (Sejr et al., 2017). Freshwater-induced
121 stratification has also been shown to create vertical gradients in pCO_2 and pH with important
122 implications for flux calculations (Miller et al., 2019). Finally, Bates et al. (2014) demonstrated
123 that sea ice meltwater and melt ponds exhibit extreme variability in pCO_2 (<10 to >1500 μatm)
124 and pH (6.1 to >10.8), highlighting the complex chemical landscape of ice-influenced waters.
125 Together, these studies underscore the high spatial and temporal variability of carbonate
126 chemistry in freshened waters across the Arctic.

127 To project future CO_2 uptake or outgassing in the Arctic, we must better understand the physical
128 and chemical drivers of near-surface carbonate variability. In this study, we investigate the
129 vertical and temporal variations in pCO_2 in a stratified Arctic fjord during sea ice breakup. By
130 combining water-column pCO_2 profiles with micrometeorological flux measurements across the
131 transition from ice-covered to open water, we evaluate the applicability of the bulk flux model
132 under Arctic seasonal transitions.

133



134

135 **Figure 1.** Schematic illustrating the interface between the air and the water in conjunction with
136 pCO₂ concentration gradients. In equation 1, the concentration gradient is assumed to occur in the
137 diffusive layer between the air and water, and the concentrations are assumed to be vertically
138 constant in the turbulent layers. (Adapted from Liss and Slater, 1974; Wanninkhof et al., 2009)

140 2. Study Site and Measurement Methods

142 2.1 Study Site

143 This study was conducted in Young Sound, a high Arctic fjord system located near the Daneborg
144 Research Station in Northeast Greenland (Fig. 2). The fjord system comprises the Tyrolerfjord
145 (inner fjord) and Young Sound (outer fjord), extending approximately 90 km from Tyroler River
146 to the Greenland Sea. A sill at about 45 m depth separates Young Sound from the open ocean.
147 Young Sound is 2 to 7 km wide, with an average depth of 100 m (maximum 350 m), and a total
148 surface area of ~390 km². Tidal amplitudes range from 0.8 to 1.5 m, with mean current velocities
149 of approximately 2 cm s⁻¹ (Rysgaard et al., 2003). Freshwater inputs are primarily derived from
150 Greenland Ice Sheet runoff, local glaciers, precipitation, and snowmelt from adjacent ice-free
151 terrain. The drainage basin of the Tyrolerfjord/Young Sound system spans 2846 km², of which
152 33% is glaciated.

153
154 Sampling was conducted from 12 to 31 July 2017. Sampling occurred during and immediately
155 after a period of sea ice breakup. On 15 July, ice coverage was approximately 30%, decreasing to
156 less than 10% by 16 July. Water sampling was conducted both from an inflatable boat and via
157 sea ice leads, all in close proximity to the Greenland Ecosystem Monitoring (GEM) program's
158 standard station (Fig. 2).

160 2.2 pCO₂ Measurements Using the HydroC Sensor

161 Surface water pCO₂ was measured with a CONTROS® HydroC CO₂ sensor, which utilizes a
162 membrane equilibrator coupled with a non-dispersive infrared detector. The instrument is
163 equipped with a built-in water pump that provides flow rate of 35 ml s⁻¹ across the membrane. At
164 each sampling depth, the sensor was allowed to equilibrate for 10 to 20 minutes, and values were
165 recorded once stable for at least two minutes. The sensor operates over a range of 200-1000 µatm
166 and temperatures of -2 to 35°C. Annual calibration has been conducted using a certified 400 ±
167 2% ppm CO₂ gas that was traceable to WMO standards. The sensor showed remarkable stability
168 (397-401 ppm), supporting a measurement uncertainty of ± 2 µatm.

170 2.3 pCO₂ Estimation from TA and DIC

171 In addition to direct measurements, pCO₂ was calculated from total alkalinity (TA) and dissolved
172 inorganic carbon (DIC) using the Seacarb package (Gattuso et al., 2024) in R. Due to the low
173 salinity and cold temperatures characteristic of Arctic coastal waters, no universally accepted set
174 of equilibrium constants (K1 and K2) exists. For consistency with previous studies in the region
175 (Henson et al., 2023), we used the refitted constants from (Lueker et al., 2000). The selection of

176 equilibrium constants introduces assumptions regarding seawater composition. (Raimondi et al.,
177 2019) showed that different constants can lead to discrepancies between measured and calculated
178 pCO₂ values, ranging from -3.1 to -35.8 μatm, with Lueker et al. (2000) demonstrating the best
179 internal consistency under polar conditions. Still, (Sulpis et al., 2020) found that the calculation
180 of pCO₂ from DIC and TA can lead to uncertainty up to 15% under cold conditions, which is far
181 greater than when pCO₂ is measured directly.

182

183 **2.4 Sea Ice TA and DIC Sampling**

184 TA and DIC in sea ice were assessed using three ice cores. Each core was sectioned into 5-10 cm
185 segments and sealed in gas-tight NEN/PE bags with sampling valves (Hansen et al., 2000).
186 Samples were transported in thermally insulated boxes to a nearby field laboratory. Cold (1°C)
187 deionized water of known mass and carbonate composition (10 - 30 ml) was added to each bag,
188 which was then resealed after removing air and weighted.

189

190 The samples were melted in the dark over ~48 hours. Meltwater was transferred to 12 mL
191 Exetainer vials (Labco, UK) pre-dosed with 20 μl of saturated HgCl₂ solution (5% w/v) to
192 prevent microbial alteration. DIC was measured by on Apollo SciTech®'s AS-C3 analyzer while
193 TA was determined via potentiometric titration on an Apollo SciTech AS-ALK2 total alkalinity
194 titrator (Haraldsson et al., 1997).

195

196 **2.5 Physical Parameters**

197 Vertical profiles of conductivity, temperature, and depth (CTD) were obtained using a Seabird®
198 SBE19plus CTD. On 16 July 2017, additional surface conductivity measurements were taken
199 using a Thermo Orion-Star® instrument with an Orion 013610MD conductivity cell. Surface
200 water temperatures were independently measured with a Testo® thermometer.

201

202 **2.6 Historical Data**

203 For contextual comparison, pCO₂ time series data from the Greenland Ecosystem Monitoring
204 program are also included in the analysis. pCO₂ data from 2007-2023 was measured using the
205 same HydroC CO₂ sensor in August each year.

206

207 **2.7 Eddy Covariance**

208 Air-sea CO₂ fluxes, as well as sensible and latent heat fluxes, were estimated using
209 micrometeorological instrumentation mounted on a 3-meter mast positioned approximately 0.5
210 meters from the waterline. CO₂ concentrations were measured with a LI-COR® 7500 open-path
211 gas analyzer, and three-dimensional wind vectors were recorded using a METEK® uSonic-
212 Scientific sonic anemometer. The open-path analyzer was used at the time due to its low power
213 consumption, suitable for operation on battery systems in remote Arctic environments.

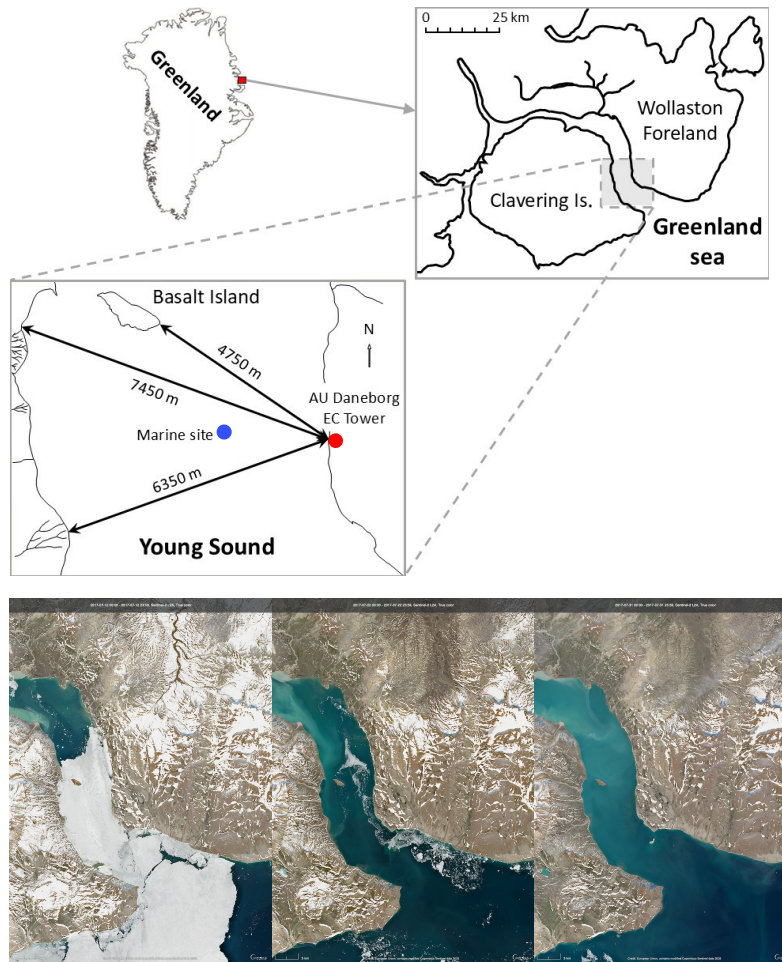
214 However, the authors recognize that open-path sensors over polar, marine environments can lead
215 to larger errors due to the cross-sensitivity between humidity and CO₂ for near infrared gas

216 analyzers (Blomquist et al., 2014; Landwehr et al., 2014). As a result, we do not aim to precisely
217 constrain CO₂ flux magnitudes throughout the study but provide support for the profiles
218 measured throughout this seasonal transition.

219
220

221 To enhance reliability, we applied three complementary analysis techniques for flux estimation:
222 (1) the standard eddy covariance (EC) method using EddyPro software (Version 7.0.6, LI-COR
223 Inc., 2019); (2) the dissipation technique (DT) (Sørensen and Larsen, 2010); and (3) the ogive
224 optimization method (OGM) (Sievers et al., 2015a). Among these, the OGM was deemed most
225 robust due to its ability identify and filter out low-frequency noise, sensor dampening, and large-
226 scale turbulent motions that can bias flux measurements. These issues often introduce large
227 relative bias associated with flux measurement over surfaces characteristically exhibiting low
228 CO₂ fluxes, such as marine surfaces (Sievers et al., 2015b). OGM's superior ability to isolate
229 relevant turbulent scales and reduce contamination from mesoscale variability is based on the
230 accumulation and modelling of each cospectra over each 20 min averaging period (Fig. S1 and
231 S2). Uncertainty in CO₂ fluxes was estimated directly from the OGM procedure. The reported
232 values correspond to the standard error associated with the fitted ogive tail and reflect random
233 uncertainty in flux integration.

234



235
236

237 **Figure 2.** Map of Greenland and the sampling area at the coast of Young Sound in Northeast
 238 Greenland. The red circle indicates the location of the Eddy Covariance tower while the Marine
 239 sampling site (Standard Station in the Greenland Ecosystem Monitoring program) is indicated as
 240 a blue circle (74.310, -20.300). Three Copernicus Sentinel true-color images of the fjord on July
 241 12, 22, and 31 illustrate the transition between sea ice cover and open water.

242

243 **3 Data and results**

244

245 **3.1 CO₂ and Heat Fluxes**

246 Surface air-sea CO₂ fluxes were measured using micrometeorological techniques between July
 247 16 and July 31, 2017 (Fig. 3a). However, only a limited number of flux estimates passed the
 248 quality control criteria defined by OGM. This method uses a Haar wavelet analysis to assess the
 249 continuity of high-frequency CO₂ and vertical wind velocity signals, rejecting fluxes when either
 250 variable fails to meet spectral continuity thresholds. In addition to the automated filtering,
 251 manual inspection of the cospectra was performed to evaluate fluxes that were soft-flagged by
 252 the Haar analysis. Only fluxes that passed both stages of evaluation were retained for further
 253 analysis and are shown in Fig. 3a (Fig. S1).

254
255 Fluxes measured using eddy covariance (EC) were highly variable throughout the period of sea
256 ice melt, exhibiting both upward and downward fluxes. Positive values indicate net efflux of CO₂
257 from the ocean to the atmosphere, implying temporary oversaturation of surface waters with
258 respect to atmospheric CO₂. EC-based effluxes were observed during and shortly after the sea
259 ice breakup period. These estimates contrast with prior studies in Young Sound, which describe
260 the fjord as a net CO₂ sink throughout the year (Sejr et al., 2011). However, historic estimates are
261 based on pCO₂ measurements from the month of August and taken at 1 m depth; not from
262 vertical pCO₂ profiles that capture salinity gradients. Similar episodic outgassing events have
263 been documented in other Arctic coastal systems under variable sea ice conditions, though
264 particularly during or following sea ice melt (Butterworth et al., 2025; Else et al., 2011; Miller et
265 al., 2011; Papakyriakou and Miller, 2011; Prytherch and Yelland, 2021; Sievers et al., 2015c).

266
267 In addition to CO₂ fluxes, eddy covariance measurements of sensible and latent heat fluxes were
268 also quantified during the same period and are presented in Fig. 3b and 3c. For all scalar
269 quantities, negative values represent downward fluxes directed toward the ocean surface. These
270 heat flux data provide important context for interpreting variability in CO₂ exchange, as they
271 reflect changes in atmospheric forcing and surface stratification. Corresponding meteorological
272 variables, including wind speed and air temperature, are shown in Fig. 3d-f.

273
274 The flux uncertainties shown in Fig. S3 quantify random uncertainty from the OGM integration
275 procedure, and illustrate CO₂ uncertainties were typically below 5 mmol m⁻² d⁻¹. Low
276 uncertainties during both uptake and efflux events demonstrated a good signal to noise ratio and
277 provide support for the integration of fluxes during these variable conditions. The highest
278 uncertainties that exceed 5 mmol m⁻² d⁻¹ corresponded to near-zero fluxes, where precise flux-
279 estimation becomes more difficult. However, these calculated uncertainties do not account for
280 potential systematic bias related to water vapor cross sensitivity, which must be evaluated
281 through other metrics.

282
283

284 **3.2 Surface Water pCO₂**

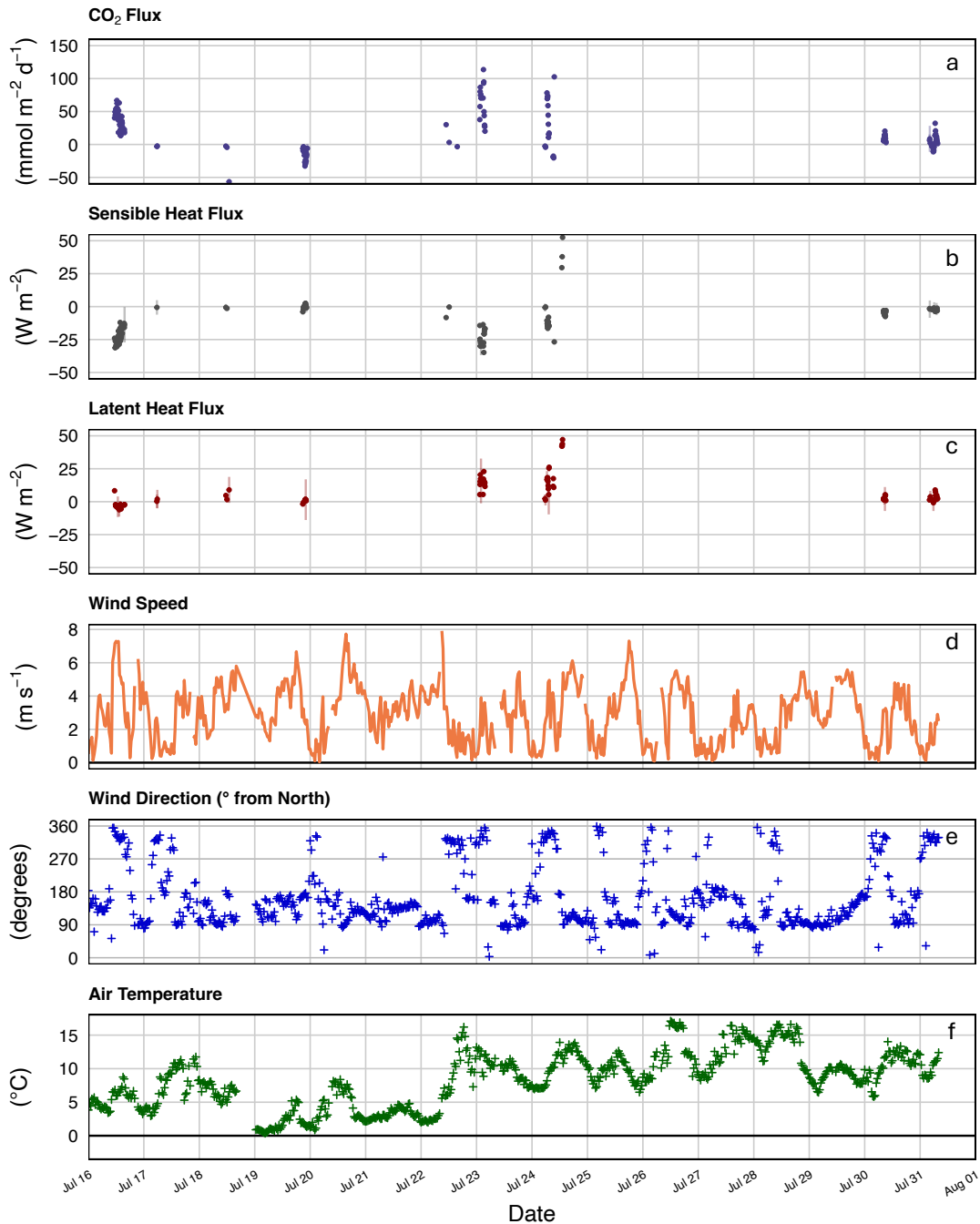
285 Vertical profiles of surface water pCO₂ were measured using the CONTROS® HydroC CO₂
286 sensor across three distinct periods in July 2017 (Fig. 5a-c). Each observational period
287 corresponded to different sea ice conditions: before, during and after sea ice breakup (Fig. 2).
288 These high-resolution profiles revealed substantial vertical variability within the upper 2 to 3
289 meters of the water column. Under ice-covered conditions, pCO₂ measurements were taken
290 through an open melt pond. At this time, elevated CO₂ concentrations were observed at the very
291 surface (0.1 m), followed by a sharp decrease to approximately 1 meter depth, coinciding with
292 the ice-water interface. Below this depth, pCO₂ increased again, though remained well below
293 atmospheric concentrations (Fig. 4a).

294
295 During the period of sea ice breakup, when ice coverage ranged from approximately 30% to
296 10%, the vertical distribution of pCO₂ exhibited a similar structure. Concentrations were highest
297 near the surface, declined to a local minimum at 1 to 2 meters, and then stabilized below 3
298 meters (Fig. 4b). Following, the complete breakup of sea ice, pCO₂ showed a more gradual
299 decrease from the surface down to about 3 meters, beneath which concentrations remained
300 relatively constant (Fig. 4c). Across all three observational periods, a shallow surface layer
301 approximately 5 m thick was identified, within which most of the pCO₂ variability occurred.
302 Below this depth, pCO₂ remained relatively constant.

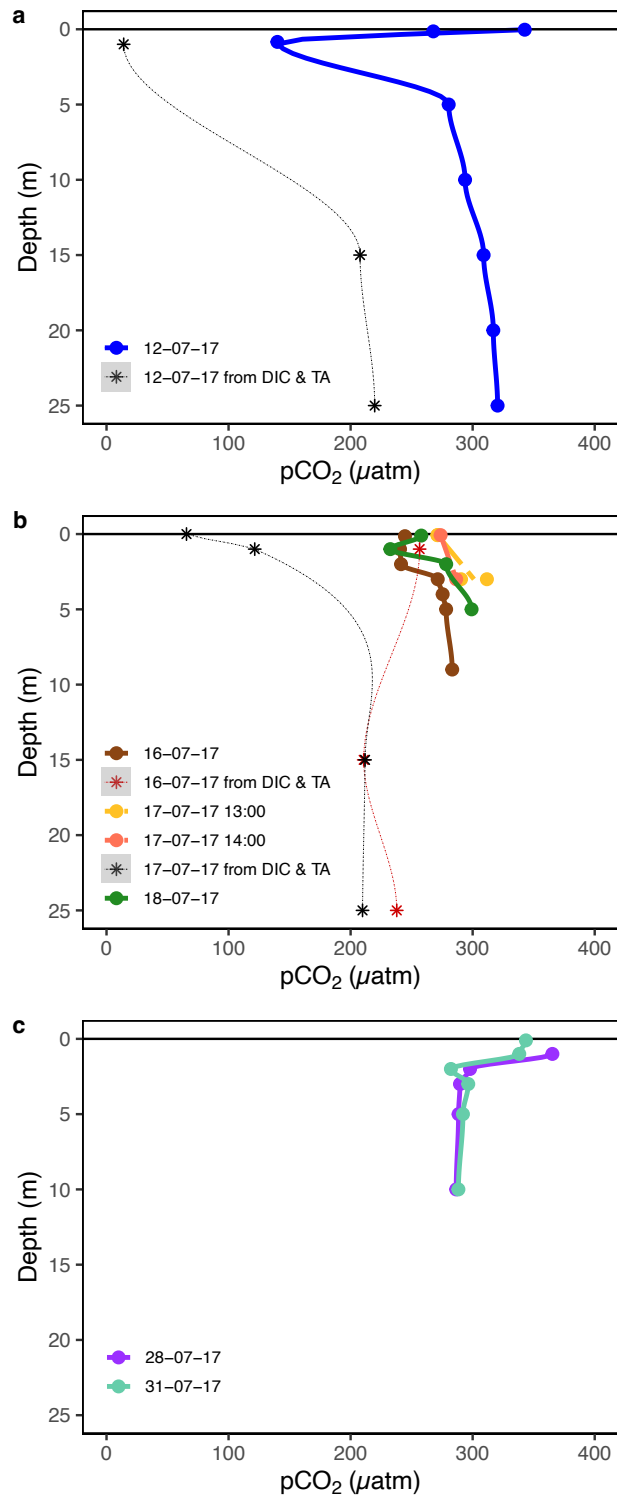
303
304 These vertical structures are consistent with strong physical stratification, likely driven by
305 freshwater input from glacial melt and surface heating. Temperature and salinity profiles
306 collected concurrently support the presence of sharp vertical gradients in the upper water
307 column, with salinity ranging from 1.4 to 29.6 PSU and temperature from -0.4°C to 6.2°C. These
308 physical profiles, shown in Fig. 5, confirm that vertical mixing was strongly suppressed during
309 the observational period.

310
311 Measurements from a different fjord in East Greenland on June 4, 2025, revealed strikingly
312 similar vertical pCO₂ heterogeneity (Fig. 6). Elevated pCO₂ at 0.1 m decreased to a minimum
313 around 1-1.5 m before increasing again and stabilizing near 3 m depth. Extreme stratification in
314 the upper few meters caused pCO₂ levels in each profile to vary by more than 100 μatm between
315 the surface and 1 m. This repeated observation of comparable vertical pCO₂ heterogeneity 8
316 years later and in a different fjord system suggest this is not an isolated phenomenon. Indeed,
317 Arctic surface stratification induces chemical changes that may influence the way we estimate
318 air-sea exchange of CO₂.

319



320
 321 **Figure 3.** The 5 min averages of measured fluxes and meteorological conditions over Young
 322 Sound during July 2017. This time period reflects the transition between sea ice break up (30%
 323 ice cover) and open water (no sea ice present) from 16 July 2017 to 1 August 2017. Air-sea
 324 exchange of (a) CO₂ (b) sensible heat and (c) latent heat were estimated using the ogive
 325 optimization method with estimated uncertainty shown as vertical error bars. (d) Wind speed, (e)
 326 wind direction and (f) air temperature are shown for the same period. Note: Use of an undried
 327 air-stream in the open-path CO₂ sensor likely inflates the magnitude of the illustrated CO₂ fluxes
 328 due to water vapor cross sensitivity.

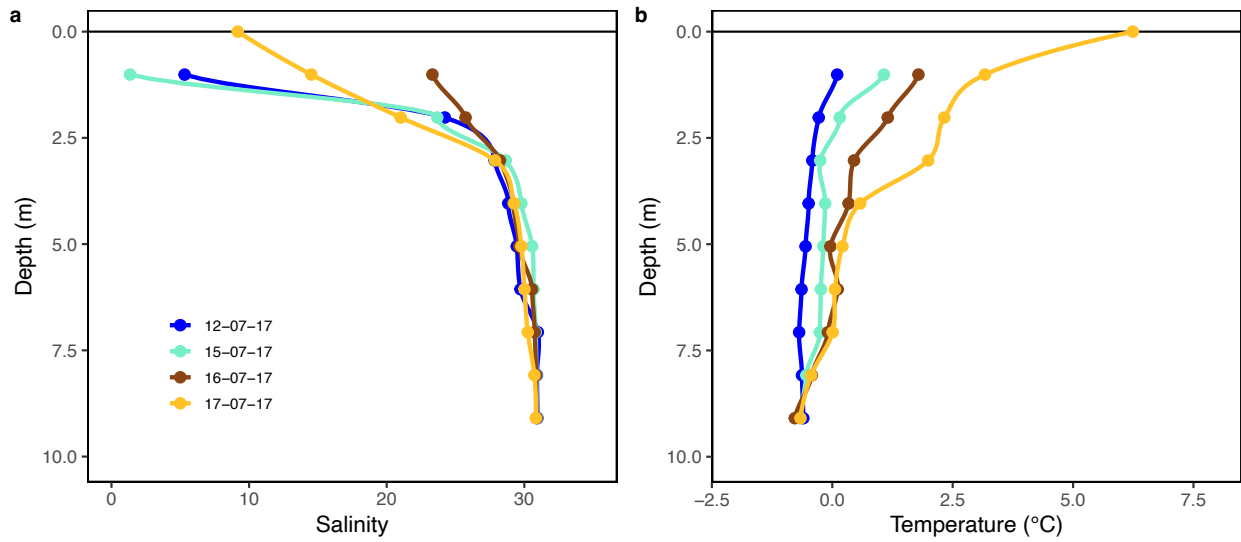


330

331

332 **Figure 4.** Measured Young Sound $p\text{CO}_2$ profiles (a) prior to sea ice breakup (measured through
 333 open melt pond), (b) during sea ice breakup and (c) after sea ice break up measured through CO_2
 334 equilibration and calculation from carbonate chemistry parameters (DIC & TA).

335

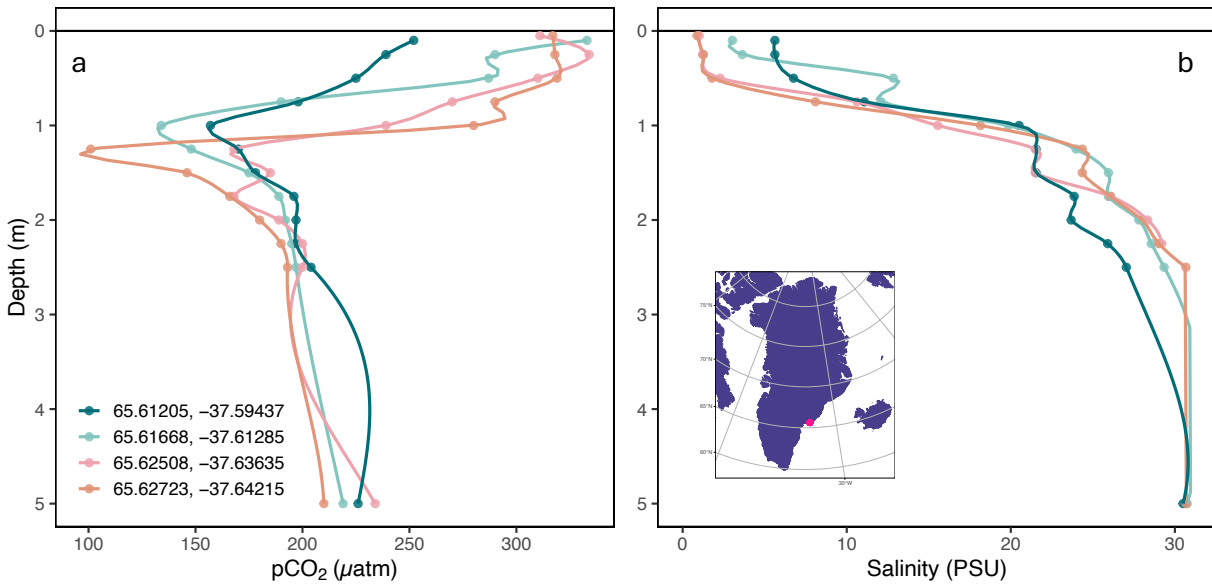


336

337

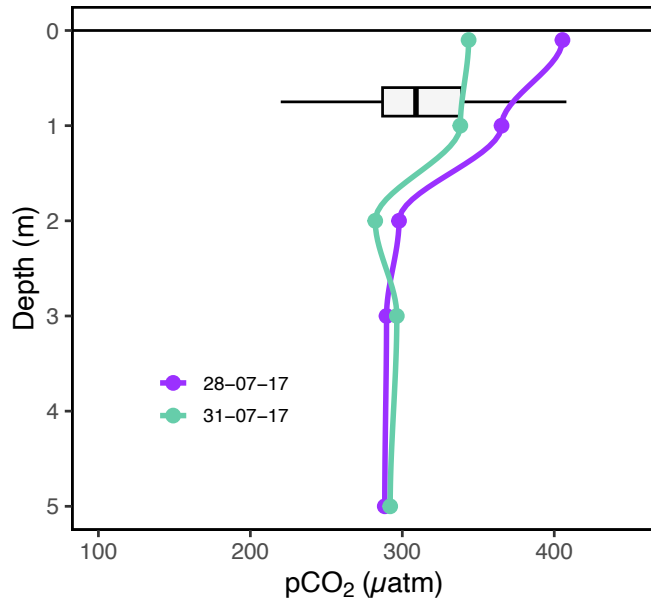
338 **Figure 5.** Measured Young Sound profiles of under-ice water and open water salinity and
339 temperature.

340



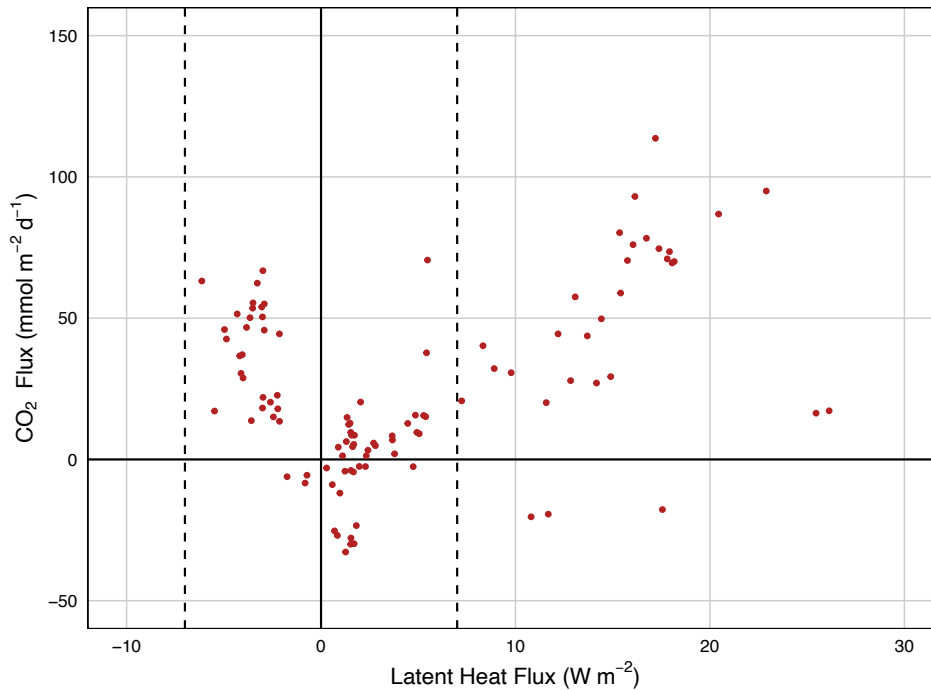
341

342 **Figure 6.** Measured pCO₂ (a) and salinity (b) profiles at 4 locations in Tasiilaq Bay. Profiles
343 were measured on June 4, 2025 following the method in Sejr et al. (2011).



344
345
346
347
348

Figure 7. Measured Young Sound pCO₂ profile after ice break up in 2017 compared with historical variation in pCO₂ at 1 m depth in the same location.



349
350
351
352
353
354
355

Figure 8. Relationship between CO₂ and latent heat fluxes measured using eddy covariance. Vertical dotted lines delineate the threshold ($|LE| < \sim 7 \text{ W m}^{-2}$) where Landwehr et al. (2014) found negligible water vapor-related biases in measurements from the un-dried infrared gas analyzer. Data within this range demonstrate both CO₂ uptake and effluxes, indicating that air-sea CO₂ exchange may change direction during the dynamic period of sea ice melt.

356
357
358
359
360
361
362
363
364
365
366
367
368
369
370
371
372
373
374
375
376
377
378
379
380
381
382
383
384
385
386
387
388
389
390
391
392
393
394
395

4. Discussion

Air-sea CO₂ fluxes in Arctic coastal areas are generally estimated using bulk parameterization models (Henson et al., 2024; Meire et al., 2015; Roobaert et al., 2019; Sejr et al., 2011). These models rely on several key assumptions, including unstratified surface conditions, a linear pCO₂ gradient within the diffusive boundary layer, and a vertically uniform pCO₂ profile within the mixed layer. Our observations challenge the applicability of these assumptions in Arctic coastal waters in several important ways.

4.1. Evaluating the Constant pCO₂ Assumption

Vertical pCO₂ profiles collected during July 2017 revealed pronounced non-linear behavior in the upper 3 to 5 meters of the water column (Fig. 4). This directly contradicts the assumption that the $\Delta p\text{CO}_2$ accurately represents the difference between the atmosphere and the “well-mixed bulk fluid” below the diffusive layer (Wanninkhof et al., 2009). Under ice-covered conditions, the lowest pCO₂ values (~150 ppm) were consistently observed just beneath the sea ice, with concentrations increasing with depth and stabilizing around 5 m (Fig. 4a). During the ice breakup stage, a similar pattern emerged, although the minimum pCO₂ was higher (~250 ppm).

More recent measurements from Tasiilaq Bay in June 2025 demonstrate very similar vertical pCO₂ profiles. Indeed, 4 high-resolution profiles with measurements every 0.25 m reveal the same C-shaped pCO₂ variation. Like in Young Sound, the most elevated pCO₂ levels were observed near the surface, and pCO₂ minimums occurred near 1-2 meters depth before increasing and becoming stable. This repeated observation in a different fjord system, but during the period of sea ice breakup indicates this vertical variability may be representative during stratified Arctic conditions.

Several interacting processes influence surface water chemistry during ice breakup. Low surface water pCO₂ values reflect the influence of low-salinity meltwater from snow and sea ice or glacial meltwater found in freshened Arctic waters (Geilfus et al., 2015; Henson et al., 2025). However, surface water chemistry during the ice breakup period is further complicated by processes such as ikaite (CaCO₃·6H₂O) dissolution (Miller et al., 2011; Rysgaard et al., 2013; Søgaard et al., 2013) and high under-ice primary production (Søgaard et al., 2021). Additionally, snowmelt, characterized by low pH and ionic strength (de Caritat et al., 2005), may further alter carbonate system dynamics in the upper water column.

Two mechanisms may explain the nonlinear C-shaped trend in pCO₂ observed in the top few meters. First, as demonstrated by Henson et al. (2025) mixing between glacial meltwater and seawater can result in nonlinear behavior in pCO₂, even when DIC and TA mix conservatively. In such cases, initial freshwater dilution leads to dramatically reduced pCO₂, but at very low salinities, the diminished buffering capacity can cause acidification to occur and pCO₂ to

396 increase again. Although, Henson et al. focused on glacial meltwater, our results suggest similar
397 processes could occur in systems influenced by sea ice and snowmelt.

398
399 Both glacial meltwater and sea ice have low DIC concentrations and act to dilute the inorganic
400 carbon of the surface ocean (Fig. S4). However, changes in alkalinity can also impact the
401 buffering capacity of the water mixture, leading to nonlinear effects. If the meltwater has a lower
402 TA:DIC ratio than seawater, due to the absence of ikaite, acidification and a shift in carbonate
403 equilibria at very low salinities could lead to higher pCO₂ values at the surface. During July
404 2017, Young Sound showed both diluted DIC and TA levels in upper few meters, suggesting pH
405 change during sea ice break up could occur more easily (Fig. S4). Indeed, calculated pH profiles
406 indicated variable surface conditions between periods of sea ice cover and sea ice breakup (Fig.
407 S5). In this very fresh surface layer, diminished pH may elevate pCO₂ relative to waters around 1
408 m depth, where freshwater-seawater mixing ratios are more moderate and seawater buffering
409 leads to very low CO₂ concentrations.

410
411 A second, but less likely, explanation involves atmospheric equilibration of sea ice melt ponds
412 before draining into open leads. The relatively elevated pCO₂ observed at ~0.1 m depth could
413 reflect such partial equilibration. While chamber-based studies (e.g. Geilfus et al., 2012, 2015;
414 Nomura et al., 2010; Semiletov et al., 2004) have demonstrated both uptake and efflux of CO₂ in
415 melt ponds, equilibrium times between melt-pond water and atmosphere depend upon pond
416 depth, wind speed, and carbonate chemistry. For example, a 0.1 m deep pond under low wind
417 conditions (~2 m s⁻¹) may reach atmospheric equilibrium in 1-4 days. However, in our case,
418 pCO₂ values calculated from TA and DIC in melt ponds did not indicate equilibrium with the
419 atmosphere, making this explanation less likely than the freshwater mixing mechanism.
420 Nevertheless, atmospheric equilibration may play a role after the sea ice barrier is removed.
421 Elevated pCO₂ levels at the surface (0.1 m) post sea ice breakup may result from the
422 combination of the chemical changes described above and from atmospheric CO₂ uptake (partial
423 equilibration) in the limited volume of this freshwater lens.

424
425 As melt progresses and sea ice recedes, riverine input and vertical mixing become more
426 influential. Yet even after ice breakup, surface waters often remain fresh due to glacial meltwater
427 runoff, and the resulting low salinities help maintain stratification. In August 2017, vertical
428 structure remained pronounced, with elevated pCO₂ at 0.1 m which stabilized below ~3 m. In
429 other words, near-surface conditions remained decoupled from deeper waters. This persistent
430 shallow layer, characterized by low salinity, higher temperature, and elevated pCO₂, suppresses
431 gas exchange with the colder, more undersaturated water below, consistent with observations by
432 Dong et al. (2021). In such environments, bulk flux models that assume homogeneity and linear
433 gradients are likely to yield biased or inaccurate estimates.

434 To place these 2017 measurements in historical context, we examined long-term surface water
435 pCO₂ data collected at 0.5-1 m depth by the Greenland Ecosystem Monitoring (GEM) program

436 between 2007 and 2023. These data, measured using consistent protocols, are presented in Fig. 7
437 alongside our open-water profiles. Over the 17-year record, August pCO₂ concentrations at ~1 m
438 depth had ranged from 220 to 408 μatm and had consistently remained below atmospheric levels.
439 This apparent stability has contributed to the perception of sustained CO₂ uptake throughout the
440 summer season.

441 However, the high-resolution vertical profiles obtained during the 2017 field campaign challenge
442 this assumption. Elevated pCO₂ levels confined to the uppermost meter of the water column may
443 go undetected in standard monitoring approaches that rely on fixed-depth sampling. These
444 results suggest that short-lived episodes of CO₂ outgassing can occur during rapid environmental
445 transitions such as sea ice breakup. Consequently, existing sampling protocols may
446 underestimate surface variability and bias flux estimates, especially in stratified conditions where
447 near-surface chemistry is decoupled from subsurface layers.

448

449 **4.2. Evaluating Bulk Model Flux Estimates**

450 To assess whether bulk models are suitable for estimating CO₂ fluxes in an Arctic fjord
451 influenced by sea ice and snow melt, we calculated fluxes using seawater pCO₂ measurements
452 from multiple depths and two gas transfer velocity parameterizations. Specifically, we computed
453 fluxes throughout July using pCO₂ measured at 0.1, 1, 2, and 4 m. To estimate the surface
454 (interface) pCO₂ at 0 m, we adjusted the 1 m pCO₂ measurements to a derived skin temperature
455 (Table 1), estimated from sensible heat fluxes (Fig. 3b) following the parameterization of
456 Smedman et al. (2007). Accounting for this skin layer correction is critical, as Woolf et al.
457 (2016) demonstrated that neglecting the thermal skin and relying only on bulk sea surface
458 temperature can introduce significant errors in flux estimates.

459

460 The resulting calculations (Table 1) show that estimated CO₂ fluxes vary significantly depending
461 on the depth of the pCO₂ measurement. Notably, fluxes derived from 0.1 m differ markedly from
462 those based on deeper values. Since many studies rely on pCO₂ measured at a fixed depth (often
463 at 1 m or at a ship's seawater intake below 5 m), these results underscore the potential for
464 misrepresentation of flux direction and magnitude due to vertical heterogeneity in surface water
465 chemistry.

466

467 Measured fluxes from eddy covariance (Fig. 3a) also exhibited large temporal variability. While
468 micrometeorological methods integrate fluxes over a horizontal footprint, bulk flux models rely
469 on single point pCO₂ gradients between air and water. Consequently, under heterogeneous or
470 partially ice-covered conditions, the two methods are unlikely to yield identical results.

471 However, a qualitative comparison between the two approaches remains informative. Notably,
472 agreement between micrometeorological and bulk model estimates was only observed in late
473 July, and only when in situ pCO₂ was normalized to the derived skin temperature. This aligns
474 with the conclusions of Woolf et al. (2016) and Ford et al. (2024), who suggest that using skin-
475 adjusted pCO₂ may improve flux estimates. Accurate application of this correction would require

476 either direct measurements of skin temperature when sampling for the bulk method or high-
477 resolution modeling of heat fluxes.

478
479 However, this agreement between methods did not hold before or immediately after ice breakup.
480 During these periods, micrometeorological methods indicated episodes of large upward fluxes,
481 while bulk model estimates suggested downward fluxes ($-14 \text{ mmol m}^{-2} \text{ d}^{-1}$). Although both
482 methods yielded comparable magnitudes for downward fluxes, only the micrometeorological
483 approach captured large upward events that could not be reconciled with surface water pCO_2
484 profiles alone.

485
486 Measurements from both Young Sound and Tasiilaq demonstrate that during sea ice breakup,
487 pCO_2 levels are most elevated at the surface. This may be linked to acidification of the most
488 freshened 0.5 m and a shift in the marine carbonate system, or partial equilibration due to air-sea
489 gas transfer. If this acidified freshwater lens warms, for instance, due to solar radiation, pCO_2
490 may rise leading to oversaturation relative to atmospheric concentrations. Indeed, when pCO_2
491 measurements on July 31 were corrected for skin temperature, to estimate pCO_2 at the boundary
492 layer, they suggested a transition from undersaturation to oversaturation (Table 1). While we did
493 not directly observe this oversaturation in the vertical profiles, this likely reflects the inability to
494 sample at the very surface layer. Moreover, profile measurements represent only single points in
495 a system characterized by strong spatial and temporal variability during this seasonal transition.
496 Nevertheless, the occurrence of C-shaped pCO_2 profiles during sea ice breakup may help explain
497 the apparent reversal of flux direction suggested by the micrometeorological approach.

498
499 Another potential explanation for the elevated CO_2 efflux that cannot be discounted involves
500 cross-sensitivity between water vapor and CO_2 in open-path NDIR sensors (Blomquist et al.,
501 2014; Landwehr et al., 2014). Although the OGM processing method is designed to minimize
502 humidity-induced artifacts and large-scale turbulent motions, it cannot entirely remove them.
503 While many of the extreme eddy covariance measurements from Young Sound are likely
504 influenced by humidity- CO_2 cross sensitivity, several lines of evidence indicate that some
505 positive CO_2 fluxes may not solely be attributed to this artifact.

506 In their comparative methodological study, Landwehr et al. (2014) identified large biases in
507 open-path NDIR sensors related to water-vapor fluctuations, but reported agreement between
508 sensors operating with dried and undried air streams during periods of low latent heat flux ($|\text{LE}|$
509 $\leq 7 \text{ W m}^{-2}$), where humidity-related bias was negligible. When examining the subset of Young
510 Sound data below this threshold, eddy covariance measurements exhibit both positive and
511 negative CO_2 flux estimates (Fig. 8). Additionally, elevated CO_2 concentrations occur across a
512 wide range of relative humidities (Fig. S6) Taken together, these patterns support the
513 interpretation that some of the measured effluxes may represent real air-sea CO_2 exchange rather
514 than solely resulting from cross-sensitivity artifacts. However, definitive quantification using this
515 experimental setup remains impossible and future studies using closed-path sensors during

516 Arctic seasonal transitions are required to robustly constrain the magnitude of CO₂ outgassing
517 and uptake.

518
519 Overall, these findings echo those of Miller et al. (2019), who reported pronounced spatial
520 heterogeneity in Arctic coastal pCO₂ and large differences in estimated flux depending on the
521 sampling depth. The broader implications of this heterogeneity for seasonal or regional flux
522 estimates remain unclear. However, if fluxes are upscaled from sparse, single-point
523 measurements (e.g., once per month, as in Laruelle et al., 2014), substantial errors may result due
524 to unrecognized spatial and temporal variability. Thus, our results emphasize the need for
525 continuous, high-resolution observations of air-sea CO₂ fluxes, particularly in Arctic coastal
526 systems affected by stratification and meltwater input. These observations will be essential for
527 refining flux parameterizations, reducing uncertainty in carbon budget estimates, and improving
528 the representation of Arctic shelf systems in global carbon models.

529
530 **Table 1.** CO₂ fluxes calculated based on pCO₂ measured at the different depth. The fluxes are
531 calculated using the bulk model of Ho et al., 2006 and Nightingale et al. (2000). We have used
532 locally measured wind speeds for the calculations to match flux measurements captured by eddy
533 covariance.

534

Date	Depth (m)	Temperature (°C)	Salinity (psu)	pCO ₂ (µatm)	Wind Speed (m s ⁻¹)	Ho (2006)	Nightingale (2000)	Eddy Covariance
						Flux (mmol CO ₂ m ⁻² day ⁻¹)	Flux (mmol CO ₂ m ⁻² day ⁻¹)	Flux (mmol CO ₂ m ⁻² day ⁻¹)
16-Jul	0.0	3.0 [†]	23	252 [‡]	6.8	-14.88	-13.69	48.3
16-Jul	0.1	3.0	23	244	6.8	-15.78	-14.52	
16-Jul	1.0	1.8	26	240	6.8	-16.12	-14.83	
16-Jul	2.0	1.1	28	241	6.8	-15.93	-14.66	
16-Jul	4.0	0.3	29	275	6.8	-12.19	-11.21	
18-Jul	0.0	6.0 [†]	7	262 [‡]	3.3	-3.45	-3.38	-3.49
18-Jul	0.1	4.3	7	244	3.3	-3.98	-3.90	
18-Jul	1.0	3.2	14	233	3.3	-4.20	-4.11	
18-Jul	2.0	2.3	21	278	3.3	-2.86	-2.79	
18-Jul	4.0	0.6	29	295	3.3	-2.34	-2.29	
28-Jul	0.0	10.0 [†]	15	415 [‡]	2.5	0.53	0.54	—
28-Jul	0.1	10.0	15	405	2.5	0.38	0.38	
28-Jul	1.0	7.0	21	365	2.5	-0.22	-0.23	
28-Jul	2.0	5.0	27	282	2.5	-1.43	-1.45	
28-Jul	4.0	2.0	30	290	2.5	-1.32	-1.34	
31-Jul	0.0	12.0 [†]	15	401 [‡]	2.0	0.20	0.21	5.07
31-Jul	0.1	10.0	15	343	2.0	-0.36	-0.38	
31-Jul	1.0	8.0	21	338	2.0	-0.40	-0.42	
31-Jul	2.0	5.0	27	282	2.0	-0.92	-0.97	
31-Jul	4.0	2.0	30	294	2.0	-0.81	-0.85	

535

536 † Denotes skin temperatures derived from heat fluxes. ‡ Denotes pCO₂ values estimated from
537 measurements at 1 m depth and adjusted to derived skin temperatures.

538

539

540 **5 Conclusions**

541

542 During the summer thaw, carbon chemistry and pCO₂ dynamics in Arctic coastal surface waters
543 are significantly altered by the combined effects of snow and sea ice melt, terrestrial runoff, and
544 biological activity. These influences lead to substantial variability in surface temperature, pH,
545 dissolved inorganic carbon (DIC), and total alkalinity (TA), ultimately disrupting carbonate

546 system equilibrium in the upper water column. As a result, estimating air-sea CO₂ fluxes using
547 traditional bulk models becomes highly uncertain during this period.

548
549 The sea ice breakup period, typically lasting 2-4 weeks, represents a particularly dynamic and
550 complex phase in the annual cycle. Despite its brevity, this phase may have a disproportionate
551 influence on total summer CO₂ uptake, given that open-water conditions in high Arctic fjords are
552 limited to only 80-120 days per year (Sejr et al., 2011).

553
554 Improved flux estimates will require more detailed and spatially resolved investigations aimed at
555 developing and validating gas exchange parameterizations tailored to the highly stratified and
556 ice-affected conditions of Arctic fjords. In particular, new approaches are needed to estimate gas
557 transfer velocities over waters influenced by snow and sea ice melt. Exchange rates depend not
558 only on the pCO₂ gradient between the atmosphere and surface water, but also on rapid,
559 nonlinear changes in surface water chemistry driven by the composition and volume of
560 meltwater and runoff.

561
562 Once more suitable parameterizations for gas transfer velocity are established, accurate flux
563 estimation will also require knowledge of the depth at which surface water pCO₂ becomes
564 vertically homogeneous. Profiling pCO₂ in the upper water column is therefore essential to
565 identify this depth and to constrain surface flux estimates reliably.

566
567 Several eddy covariance studies in other arctic environments report variable uptake and efflux of
568 CO₂ during the sea ice breakup period (e.g. Butterworth et al., 2025). Similarly, eddy covariance
569 measurements in Young Sound exhibited both positive and negative CO₂ flux estimates during
570 this seasonal transition. However, these upward fluxes were not captured by the bulk model.
571 These variable and sometimes conflicting datasets underscore the need for studies that integrate
572 continuous, direct CO₂ flux measurements with detailed observations of surface water carbonate
573 chemistry, atmospheric forcing, skin temperature, and turbulence at the air-ice-water interface.

574
575 Such integrated measurements are critical to improving our understanding of the frequency,
576 drivers, and net effect of episodic upward CO₂ fluxes in Arctic coastal systems. Ultimately, this
577 knowledge is essential to accurately quantify the seasonal and regional uptake of atmospheric
578 CO₂ in the rapidly changing Arctic.

579

580

581 **Acknowledgments**

582 This study is a contribution to the GreenFeedback project (Greenhouse gas fluxes and earth
583 system feedbacks, Grant agreement: 101056921), funded by the European Union under the
584 Horizon Europe program, who also supported L.L.S and H.C.H's involvement. H.C.H. was
585 additionally funded by the AUFF (Aarhus Universitets Forskningsfond, project no. AUFF-F-

586 2021-7-7) as part of his PhD. S.R. was funded by Aage V Jensens Fonde (grant no. AVJF21-
587 3012) and the Danish National Research Foundation (grant no. DNRF 185). MKS was funded by
588 the POMP project (Horizon Europe grant: 101136875) and the Connecting the Dots project
589 (Villum Foundation grant: 50110) D.H.S received financial support from the Greenland Climate
590 Research Centre (GCRC), Greenland Institute of Natural Resources. The study also received
591 financial support from The Danish Ministry of Climate, Energy and Utilities, Programme for
592 Arctic Climate, (project: Drivhusgas-observationer i Arktis (ObsArktis), 2017). Furthermore we
593 received support from The Arctic Research Centre, Aarhus University and Greenland Institute of
594 Natural Science. The authors especially wish to thank Egon Randa Frandsen, who assisted with
595 the logistics and the additional measurements in Young Sound. Additionally, the authors would
596 like to recognize the students in the EnCHil Nordic master program, who participated in taking
597 the Tasiilaq measurements. This work is a contribution to the Arctic Science Partnership (ASP)
598 and the MarinBasis component of the Greenland Ecosystem Monitoring Program.
599

599

600 **Author Contribution**

601 Conceptualization: LLS. Formal analysis, writing – original draft preparation: HCH. Funding
602 acquisition: LLS, SR, MKS, TP. Investigation: DS, BJ, KL, TP, MKS, JS, SR, LLS. Writing –
603 review and editing: DS, TP, MKS, SR, LLS. All the authors have read and agreed to the
604 published version of the paper.
605

605

606 **Data Availability Statement**

607 Vertical profiles from both Greenlandic fjords can be found in the Zenodo data repository:
608 <https://doi.org/10.5281/zenodo.17471918>
609

609

610 **Competing interests**

611 The authors declare no competing interests.
612

612

613

614 **References**

615

616 Ahmed, M. M. M., Else, B. G. T., Capelle, D., Miller, L. A., and Papakyriakou, T.: Underestimation of surface p
617 CO_2 and air-sea CO_2 fluxes due to freshwater stratification in an Arctic shelf sea, Hudson Bay, Elementa: Science
618 of the Anthropocene, 8, 084, <https://doi.org/10.1525/elementa.084>, 2020.

619 Arrigo, K. R. and van Dijken, G. L.: Continued increases in Arctic Ocean primary production, Progress in
620 Oceanography, 136, 60–70, <https://doi.org/10.1016/j.pocean.2015.05.002>, 2015.

621 Bates, N. R. and Mathis, J. T.: The Arctic Ocean marine carbon cycle: evaluation of air-sea CO_2 exchanges, ocean
622 acidification impacts and potential feedbacks, Biogeosciences, 6, 2433–2459, 2009.

623 Blomquist, B. W., Huebert, B. J., Fairall, C. W., Bariteau, L., Edson, J. B., Hare, J. E., and McGillis, W. R.:
624 Advances in Air–Sea CO_2 Flux Measurement by Eddy Correlation, Boundary-Layer Meteorol, 152,
625 245–276, <https://doi.org/10.1007/s10546-014-9926-2>, 2014.

- 626 Burgers, T. M., Miller, L. A., Thomas, H., Else, B. G. T., Gosselin, M., and Papakyriakou, T.: Surface Water CO₂
627 Variations and Sea-Air CO₂ Fluxes During Summer in the Eastern Canadian Arctic, *J. Geophys. Res. Oceans*, 122,
628 9663–9678, <https://doi.org/10.1002/2017jc013250>, 2017.
- 629 Butterworth, B. J., Else, B. G. T., Brown, K. A., Mundy, C. J., Williams, W. J., Rotermund, L. M., and de Boer, G.:
630 Annual carbon dioxide flux over seasonal sea ice in the Canadian Arctic, *EGU sphere*, 1–30,
631 <https://doi.org/10.5194/egusphere-2025-1802>, 2025.
- 632 de Caritat, P., Hall, G., Gislason, S., Belsey, W., Braun, M., Goloubeva, N. I., Olsen, H. K., Scheie, J. O., and Vaive,
633 J. E.: Chemical composition of arctic snow: concentration levels and regional distribution of major elements,
634 *Science of The Total Environment*, 336, 183–199, <https://doi.org/10.1016/j.scitotenv.2004.05.031>, 2005.
- 635 Dai, M., Su, J., Zhao, Y., Hofmann, E. E., Cao, Z., Cai, W.-J., Gan, J., Lacroix, F., Laruelle, G. G., Meng, F.,
636 Müller, J. D., Regnier, P. A. G., Wang, G., and Wang, Z.: Carbon Fluxes in the Coastal Ocean: Synthesis, Boundary
637 Processes, and Future Trends, *Annu. Rev. Earth Planet. Sci.*, 50, 593–626, [https://doi.org/10.1146/annurev-earth-](https://doi.org/10.1146/annurev-earth-032320-090746)
638 032320-090746, 2022.
- 639 Dong, Y., Yang, M., Bakker, D. C. E., Liss, P. S., Kitidis, V., Brown, I., Chierici, M., Fransson, A., and Bell, T. G.:
640 Near-Surface Stratification Due to Ice Melt Biases Arctic Air-Sea CO₂ Flux Estimates, *Geophysical Research*
641 *Letters*, 48, <https://doi.org/10.1029/2021GL095266>, 2021.
- 642 Else, B. G. T., Papakyriakou, T. N., Galley, R. J., Drennan, W. M., Miller, L. A., and Thomas, H.: Wintertime CO₂
643 fluxes in an Arctic polynya using eddy covariance: Evidence for enhanced air-sea gas transfer during ice formation,
644 *J. Geophys. Res.*, 116, C00G03, <https://doi.org/10.1029/2010JC006760>, 2011.
- 645 Ford, D. J., Shutler, J. D., Blanco-Sacristán, J., Corrigan, S., Bell, T. G., Yang, M., Kitidis, V., Nightingale, P. D.,
646 Brown, I., Wimmer, W., Woolf, D. K., Casal, T., Donlon, C., Tilstone, G. H., and Ashton, I.: Enhanced ocean CO₂
647 uptake due to near-surface temperature gradients, *Nat. Geosci.*, 17, 1135–1140, [https://doi.org/10.1038/s41561-024-](https://doi.org/10.1038/s41561-024-01570-7)
648 01570-7, 2024.
- 649 Garbe, C. S., Rutgersson, A., Boutin, J., de Leeuw, G., Delille, B., Fairall, C. W., Gruber, N., Hare, J., Ho, D. T.,
650 Johnson, M. T., Nightingale, P. D., Pettersson, H., Piskozub, J., Sahlée, E., Tsai, W., Ward, B., Woolf, D. K., and
651 Zappa, C. J.: Transfer Across the Air-Sea Interface, in: *Ocean-Atmosphere Interactions of Gases and Particles*,
652 edited by: Liss, P. S. and Johnson, M. T., Springer, Berlin, Heidelberg, 55–112, [https://doi.org/10.1007/978-3-642-](https://doi.org/10.1007/978-3-642-25643-1_2)
653 25643-1_2, 2014.
- 654 Gattuso, J.-P., Epitalon, J.-M., Lavigne, H., Orr, J., Gentili, B., Hagens, M., Hofmann, A., Mueller, J.-D., Proye, A.,
655 Rae, J., and Soetaert, K.: *seacarb: Seawater Carbonate Chemistry*, 2024.
- 656 Geilfus, N.-X., Carnat, G., Papakyriakou, T., Tison, J.-L., Else, B., Thomas, H., Shadwick, E., and Delille, B.:
657 Dynamics of pCO₂ and related air-ice CO₂ fluxes in the Arctic coastal zone (Amundsen Gulf, Beaufort Sea), *J.*
658 *Geophys. Res.*, 117, n/a-n/a, <https://doi.org/10.1029/2011JC007118>, 2012.
- 659 Geilfus, N.-X., Galley, R. J., Crabeck, O., Papakyriakou, T., Landy, J., Tison, J.-L., and Rysgaard, S.: Inorganic
660 carbon dynamics of melt-pond-covered first-year sea ice in the Canadian Arctic, *Biogeosciences*, 12, 2047–2061,
661 <https://doi.org/10.5194/bg-12-2047-2015>, 2015.
- 662 Granskog, M. A., Kuzyk, Z. Z. A., Azetsu-Scott, K., and Macdonald, R. W.: Distributions of runoff, sea-ice melt
663 and brine using $\delta^{18}\text{O}$ and salinity data — A new view on freshwater cycling in Hudson Bay, *Journal of Marine*
664 *Systems*, 88, 362–374, <https://doi.org/10.1016/j.jmarsys.2011.03.011>, 2011.
- 665 Hansen, J. W., Thamdrup, B., and Jørgensen, B. B.: Anoxic incubation of sediment in gas-tight plastic bags: a
666 method for biogeochemical process studies, *Marine Ecology Progress Series*, 208, 273–282, 2000.

- 667 Haraldsson, C., Anderson, L. G., Hassellöv, M., Hulth, S., and Olsson, K.: Rapid, high-precision potentiometric
668 titration of alkalinity in ocean and sediment pore waters, *Deep Sea Research Part I: Oceanographic Research Papers*,
669 44, 2031–2044, [https://doi.org/10.1016/S0967-0637\(97\)00088-5](https://doi.org/10.1016/S0967-0637(97)00088-5), 1997.
- 670 Henson, H. C., Holding, J. M., Meire, L., Rysgaard, S., Stedmon, C. A., Stuart-Lee, A., Bendtsen, J., and Sejr, M.:
671 Coastal freshening drives acidification state in Greenland fjords, *Science of The Total Environment*, 855, 158962,
672 <https://doi.org/10.1016/j.scitotenv.2022.158962>, 2023.
- 673 Henson, H. C., Sejr, M., Meire, L., Sørensen, L. L., Winding, M. H. S., and Holding, J. M.: Resolving Heterogeneity
674 in CO₂ Uptake Potential in the Greenland Coastal Ocean, *Journal of Geophysical Research: Biogeosciences*, 129,
675 e2024JG008246, <https://doi.org/10.1029/2024JG008246>, 2024.
- 676 Henson, H. C., Puts, I. C., Sejr, M. K., Sørensen, L. L., and Holding, J. M.: Glacial meltwater increases coastal
677 carbon dioxide uptake and sensitivity to biogeochemical change, *Commun Earth Environ*, 6, 687,
678 <https://doi.org/10.1038/s43247-025-02685-4>, 2025.
- 679 Jørgensen, H. E., Sørensen, L. L., and Larsen, S. E.: A Simple Model of Chemistry Effects on the Air-Sea CO₂
680 Exchange Coefficient, *Journal of Geophysical Research: Oceans*, 125, e2018JC014808,
681 <https://doi.org/10.1029/2018JC014808>, 2020.
- 682 Landwehr, S., Miller, S. D., Smith, M. J., Saltzman, E. S., and Ward, B.: Analysis of the PKT correction for direct
683 CO₂ flux measurements over the ocean, *Atmospheric Chemistry and Physics*, 14, 3361–3372,
684 <https://doi.org/10.5194/acp-14-3361-2014>, 2014.
- 685 Laruelle, G. G., Lauerwald, R., Pfeil, B., and Regnier, P.: Regionalized global budget of the CO₂ exchange at the
686 air-water interface in continental shelf seas, *Global Biogeochemical Cycles*, 28, 1199–1214,
687 <https://doi.org/10.1002/2014GB004832>, 2014.
- 688 Liss, P. S. and Slater, P. G.: Flux of Gases across the Air-Sea Interface, *Nature*, 247, 181–184,
689 <https://doi.org/10.1038/247181a0>, 1974.
- 690 Lueker, T. J., Dickson, A. G., and Keeling, C. D.: Ocean pCO₂ calculated from dissolved inorganic carbon,
691 alkalinity, and equations for K₁ and K₂: validation based on laboratory measurements of CO₂ in gas and seawater at
692 equilibrium, *Marine Chemistry*, 70, 105–119, [https://doi.org/10.1016/s0304-4203\(00\)00022-0](https://doi.org/10.1016/s0304-4203(00)00022-0), 2000.
- 693 Meire, L., Søgaard, D. H., Mortensen, J., Meysman, F. J. R., Soetaert, K., Arendt, K. E., Juul-Pedersen, T., Blicher,
694 M. E., and Rysgaard, S.: Glacial meltwater and primary production are drivers of strong
695 CO₂ uptake in fjord and coastal waters adjacent to the Greenland Ice Sheet,
696 *Biogeosciences*, 12, 2347–2363, <https://doi.org/10.5194/bg-12-2347-2015>, 2015.
- 697 Meire, L., Mortensen, J., Meire, P., Juul-Pedersen, T., Sejr, M. K., Rysgaard, S., Nygaard, R., Huybrechts, P., and
698 Meysman, F. J. R.: Marine-terminating glaciers sustain high productivity in Greenland fjords, *Glob Change Biol*, 23,
699 5344–5357, <https://doi.org/10.1111/gcb.13801>, 2017.
- 700 Miller, L. A., Papakyriakou, T. N., Collins, R. E., Deming, J. W., Ehn, J. K., Macdonald, R. W., Mucci, A., Owens,
701 O., Raudsepp, M., and Sutherland, N.: Carbon dynamics in sea ice: A winter flux time series, *J. Geophys. Res.*, 116,
702 C02028, <https://doi.org/10.1029/2009JC006058>, 2011.
- 703 Miller, L. A., Burgers, T. M., Burt, W. J., Granskog, M. A., and Papakyriakou, T. N.: Air-Sea CO₂ Flux Estimates
704 in Stratified Arctic Coastal Waters: How Wrong Can We Be?, *Geophys. Res. Lett.*, 46, 235–243,
705 <https://doi.org/10.1029/2018gl080099>, 2019.
- 706 Nomura, D., Yoshikawa-Inoue, H., Toyota, T., and Shirasawa, K.: Effects of snow, snowmelting and refreezing
707 processes on air–sea-ice CO₂ flux, *Journal of Glaciology*, 56, 262–270,
708 <https://doi.org/10.3189/002214310791968548>, 2010.

- 709 Papakyriakou, T. and Miller, L.: Springtime CO₂ exchange over seasonal sea ice in the Canadian Arctic
710 Archipelago, *Annals of Glaciology*, 52, 215–224, <https://doi.org/10.3189/172756411795931534>, 2011.
- 711 Perovich, D., Meier, W., Tschudi, M., Hendricks, S., Petty, A. A., Divine, D., Farrell, S., Gerland, S., Haas, C.,
712 Kaleschke, L., Pavlova, O., Ricker, R., Tian-Kunze, X., Webster, M., and Wood, K.: Arctic Report Card 2020: Sea
713 Ice, 2020.
- 714 Prytherch, J. and Yelland, M. J.: Wind, Convection and Fetch Dependence of Gas Transfer Velocity in an Arctic
715 Sea-Ice Lead Determined From Eddy Covariance CO₂ Flux Measurements, *Global Biogeochemical Cycles*, 35,
716 e2020GB006633, <https://doi.org/10.1029/2020GB006633>, 2021.
- 717 Raimondi, L., Matthews, J. B. R., Atamanchuk, D., Azetsu-Scott, K., and Wallace, D. W. R.: The internal
718 consistency of the marine carbon dioxide system for high latitude shipboard and *in situ* monitoring, *Marine*
719 *Chemistry*, 213, 49–70, <https://doi.org/10.1016/j.marchem.2019.03.001>, 2019.
- 720 Roobaert, A., Laruelle, G. G., Landschützer, P., Gruber, N., Chou, L., and Regnier, P.: The Spatiotemporal
721 Dynamics of the Sources and Sinks of CO₂ in the Global Coastal Ocean, *Global Biogeochemical Cycles*, 33, 1693–
722 1714, <https://doi.org/10.1029/2019GB006239>, 2019.
- 723 Rysgaard, S., Vang, T., Stjernholm, M., Rasmussen, B., Windelin, A., and Kiilsholm, S.: Physical Conditions,
724 Carbon Transport, and Climate Change Impacts in a Northeast Greenland Fjord, Arctic, Antarctic, and Alpine
725 Research, 35, 301–312, [https://doi.org/10.1657/1523-0430\(2003\)035%255B0301:PCCTAC%255D2.0.CO;2](https://doi.org/10.1657/1523-0430(2003)035%255B0301:PCCTAC%255D2.0.CO;2), 2003.
- 726 Rysgaard, S., Søgaard, D. H., Cooper, M., Pu´co, M., Lennert, K., Papakyriakou, T. N., Wang, F.,
727 Geilfus, N. X., Glud, R. N., Ehn, J., McGinnis, D. F., Attard, K., Sievers, J., Deming, J. W., and Barber, D.: Ikaite
728 crystal distribution in winter sea ice and implications for CO₂ system dynamics, *The Cryosphere*, 7, 707–718,
729 <https://doi.org/10.5194/tc-7-707-2013>, 2013.
- 730 Sejr, Krause-Jensen, D., Rysgaard, S., Sørensen, L. L., Christensen, P. B., and Glud, R. N.: Air—sea flux of CO₂ in
731 arctic coastal waters influenced by glacial melt water and sea ice, *Tellus B: Chemical and Physical Meteorology*, 63,
732 815–822, <https://doi.org/10.1111/j.1600-0889.2011.00540.x>, 2011.
- 733 Sejr, M. K., Stedmon, C. A., Bendtsen, J., Abermann, J., Juul-Pedersen, T., Mortensen, J., and Rysgaard, S.:
734 Evidence of local and regional freshening of Northeast Greenland coastal waters, *Sci Rep*, 7, 13183,
735 <https://doi.org/10.1038/s41598-017-10610-9>, 2017.
- 736 Semiletov, I., Makshtas, A., Akasofu, S., and L Andreas, E.: Atmospheric CO₂ balance: The role of Arctic sea ice,
737 *Geophysical Research Letters*, 31, 2003GL017996, <https://doi.org/10.1029/2003GL017996>, 2004.
- 738 Sievers, Papakyriakou, T., Larsen, S. E., Jammot, M. M., Rysgaard, S., Sejr, M., and Sørensen, L. L.: Estimating
739 surface fluxes using eddy covariance and numerical ogive optimization, *Atmospheric Chemistry and Physics*, 15,
740 2081–2103, <https://doi.org/10.5194/acp-15-2081-2015>, 2015a.
- 741 Sievers, J., Papakyriakou, T., Larsen, S. E., Jammot, M. M., Rysgaard, S., Sejr, M. K., and Sørensen, L. L.:
742 Estimating surface fluxes using eddy covariance and numerical ogive optimization, *Atmospheric Chemistry and*
743 *Physics*, 15, 2081–2103, <https://doi.org/10.5194/acp-15-2081-2015>, 2015b.
- 744 Sievers, J., Sørensen, L. L., Papakyriakou, T., Else, B., Sejr, M. K., Haubjerg Søgaard, D., Barber, D., and
745 Rysgaard, S.: Winter observations of CO₂ exchange between sea ice and the atmosphere in a coastal fjord
746 environment, *The Cryosphere*, 9, 1701–1713, <https://doi.org/10.5194/tc-9-1701-2015>, 2015c.
- 747 Smedman, A., Högström, U., Sahlée, E., and Cecilia, J.: Critical re-evaluation of the bulk transfer coefficient for
748 sensible heat over the ocean during unstable and neutral conditions, *Quart J Royal Meteor Soc*, 133, 227–250,
749 <https://doi.org/10.1002/qj.6>, 2007.

750 Søgaard, D. H., Thomas, D. N., Rysgaard, S., Glud, R. N., Norman, L., Kaartokallio, H., Juul-Pedersen, T., and
751 Geilfus, N.-X.: The relative contributions of biological and abiotic processes to carbon dynamics in subarctic sea
752 ice, *Polar Biol*, 36, 1761–1777, <https://doi.org/10.1007/s00300-013-1396-3>, 2013.

753 Søgaard, D. H., Sorrell, B. K., Sejr, M. K., Andersen, P., Rysgaard, S., Hansen, P. J., Skyttä, A., Lemcke, S., and
754 Lund-Hansen, L. C.: An under-ice bloom of mixotrophic haptophytes in low nutrient and freshwater-influenced
755 Arctic waters, *Sci Rep*, 11, 2915, <https://doi.org/10.1038/s41598-021-82413-y>, 2021.

756 Sørensen, L. L. and Larsen, S. E.: Atmosphere–Surface Fluxes of CO₂ using Spectral Techniques, *Boundary-Layer
757 Meteorol*, 136, 59–81, <https://doi.org/10.1007/s10546-010-9499-7>, 2010.

758 Sulpis, O., Lauvset, S. K., and Hagens, M.: Current estimates of K_1^* and K_2^* appear inconsistent with measured
759 CO₂ system parameters in cold oceanic regions, *Ocean Science*, 16, 847–862, [https://doi.org/10.5194/os-16-847-](https://doi.org/10.5194/os-16-847-2020)
760 2020, 2020.

761 Wanninkhof, R., Asher, W., Ho, D., Sweeney, C., and McGillis, W.: Advances in Quantifying Air-Sea Gas
762 Exchange and Environmental Forcing*, *Annual review of marine science*, 1, 213–44,
763 <https://doi.org/10.1146/annurev.marine.010908.163742>, 2009.

764 Watts, J., Bell, T. G., Anderson, K., Butterworth, B. J., Miller, S., Else, B., and Shutler, J.: Impact of sea ice on air-
765 sea CO₂ exchange – A critical review of polar eddy covariance studies, *Progress in Oceanography*, 201, 102741,
766 <https://doi.org/10.1016/j.pocean.2022.102741>, 2022.

767 Woolf, D. K., Land, P. E., Shutler, J. D., Goddijn-Murphy, L. M., and Donlon, C. J.: On the calculation of air-sea
768 fluxes of CO₂ in the presence of temperature and salinity gradients, *Journal of Geophysical Research: Oceans*, 121,
769 1229–1248, <https://doi.org/10.1002/2015JC011427>, 2016.

770